Light-Driven Plasmonic Color Filters by Overlaying Photoresponsive Liquid Crystals on Gold Annular Aperture Arrays

Yan Jun Liu, Guang Yuan Si, Eunice S. P. Leong, Ning Xiang, Aaron J. Danner, and Jing Hua Teng**

Plasmonics paves the way for manipulating optical signals at the nanoscale level by coupling light to coherent electronic excitations (known as surface plasmon resonances) at the dielectric/metal interface.[1] The strong confinement of light associated with surface plasmon resonances has led to the development of various subwavelength photonic components, such as waveguides,[2–4] switches,[5–7] lenses,[8–11] antennas,[12–15] and spasers.[16–19] The conversion efficiency between photons and plasmons plays the most important role in all the aforementioned components. By exploiting plasmonic nanostructures, coupling between photons and plasmons can be efficiently controlled at the subwavelength scale.[20–22] Several types of nanostructures, such as nanohole arrays,[23–26] metal–insulator–metal (MIM) structures,[26–29] and nanoslits combined with periodic grooves[30] have been used in tuning the resonant transmission peak in the visible range for potential color filtering, a crucial component for color display applications. However, issues related to these filters are low transmission due to the high loss of metals and relatively broad pass bands, which do not satisfy the requirement for the multiband spectral imaging.

Recently, noble metallic annular aperture arrays (AAAs)—plasmonic coaxial nanostructures—have drawn considerable attention due to their peculiar properties and great potential for ultracompact optical applications. Baida and coworkers have theoretically investigated the properties of the waveguiding modes in such AAAs.[31,32] The plasmon dispersion of a single coaxial structure can be conveniently engineered for various applications by controlling its coaxial geometry, composition, and surrounding dielectrics.[33,34] Atwater et al. have shown that such a single-layer coaxial nanostructure can also form metamaterials with negative refractive index in the visible range.[35,36] A distinctive property of coaxial nanostructures is that they can form a Fabry–Pérot nanocavity to support plasmonic waveguiding modes, which could lead to super-enhanced optical transmission with narrow pass bands: a characteristic feature of color filters. Experimental results have confirmed that AAAs have much higher peak transmission than simple hole arrays with the same open area.[37] Very recently, color filters based on such kind of coaxial AAAs have been demonstrated by controlling either the aperture size[38] or the aperture depth,[39] but they had low optical transmittance due to the large distance and thus weak coupling between each coaxial aperture. Furthermore, all the aforementioned AAA-based color filters are passive devices. It is much desired to develop tunable plasmonic color filters with active control and high transmittance.

Liquid crystals (LCs) are an excellent candidate for active plasmonic devices due to their wide tuning range of refractive index, high transmittance, low-power consumption, and high compatibility.[40,41] Active control of LCs has been extensively studied based on electrical, optical, and acoustical approaches.[40–43] Among these approaches, all-optical control leverages the benefits of light directed effects: remote, temporal, and spatial control. In addition, we have also reported enhanced optical transmission (>10%) from a LC-overlayed gold nanohole array.[44] In this Communication, we demonstrate a light-driven plasmonic color filter by integrating a gold AAA with photoresponsive LCs. Compared to the as-milled AAAs, the overlayed ones by the photoresponsive LCs show much higher transmittance. The effect of aperture size on the transmittance and corresponding color filtering is investigated. The optical tuning of the transmittance is performed by subjecting the device to UV flood exposure. The physical mechanisms underlying the observations are analyzed and discussed. Such a light-driven plasmonic color filter could be very useful in compact display systems and all-optical information processing.

Figure 1 shows the schematic of the sample structure and experimental setup for optical spectra measurement. The plasmonic color filter consists of a gold AAA and an overlayer of photoresponsive LC. Upon UV irradiation, the photochromic LC molecules can undergo a reversible photoisomerization between the *trans* (rodlike shape) and the *cis* (bent shape) molecular forms (see the magnified part II in Figure 1), just disrupting the local order of LC molecules and making the system optically active.

Figure 2 shows the measured absorption spectra of the *trans* and the *cis* forms of the photochromic LC, 4-butyl-4-methyoxyazobenzene (BMAB). BMAB is an azobenzene derivative, and it possesses an alkoxy substituent and a butyl group at the para positions of the azobenzene (see the inset in Figure 2). The *trans*-isomer has a main absorption band in the UV around

Dr. Y. J. Liu, Dr. E. S. P. Leong, Dr. J. H. Teng
Institute of Materials Research and Engineering
Agency for Science Technology and Research (A*STAR)
3 Research Link, Singapore 117602, Singapore
E-mail: liuy@imre.a-star.edu.sg; jh-teng@imre.a-star.edu.sg
G. Y. Si, Prof. N. Xiang, Prof. A. J. Danner
Department of Electrical and Computer Engineering
National University of Singapore
4 Engineering Drive 3, Singapore 117576, Singapore

DOI: 10.1002/adma.201104440

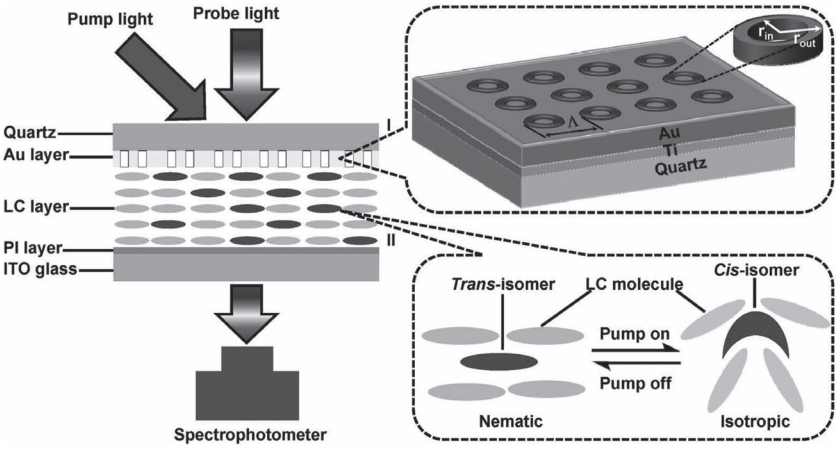

Figure 1. Schematic of the sample structure and experimental setup. The enlarged part I shows the fabricated square pattern of gold AAAs using focused ion beam lithography. The inner and outer radii of each individual aperture are labeled as r_{in} and r_{out}, respectively. The magnified part II shows the working mechanism of the optical driving process: a reversible N–I phase transition induced by the *trans–cis* photoisomerization of the photochromic LCs.

350 nm (π–π* molecular transition), whereas the *cis*-isomer has an absorption peak in the visible around 450 nm (n–π* molecular transition). The *trans*-isomer, which is the thermally stable ground state, can transform into the *cis*-isomer by absorbing UV light. Under visible light irradiation or thermal isomerisation, the *cis*-isomer can return to the *trans*-isomer form,[45] making the color filters highly reversible and reproducible.

A set of field emission scanning electron microscope (FE-SEM, ESM-9000, Elionix) images of the fabricated Au AAAs are shown in **Figure 3**a–d with varied inner radii. The whole working area of each pattern is 10 × 10 μm^2. **Figure 4**a and b show the simulated and measured transmission spectra of the plasmonic color filters with different aperture size, respectively. Compared to the as-milled AAAs (see Supporting Information (SI), Figure S1), the overlayed ones by the photoresponsive LCs show much higher transmission with prominent peaks. Note that the absorption of the BMAB was excluded in our simulation. From Figure 2, BMAB has strong absorption at wavelengths below ~480 nm, which tailors the transmission spectra of color filters. Therefore, there is a big difference in transmission intensity at short wavelengthes (below 480 nm) between Figure 4a and b. We also note that the experimental results show much higher transmission at resonant peak wavelength than the simulated results, which is mainly attributed to different references we used in the simulation and experiment. In the simulation, air was simply used as the reference, while in the experiment, a glass substrate was used as the reference. Except these two apparent discrepancies, we can see that the experimental results are in reasonable agreement with the calculations. From Figure 4a, there are two obvious transmission bands for each color filter with different aperture size: one is located in a wavelength range of 500–600 nm and the other one in 700–800 nm. They are attributed to coherent interactions between two main plasmons: cylindrical surface plasmons (CSPs) and planar surface plasmons (PSPs). CSPs strongly depend on the geometrical design and the thickness of the metal film, while PSPs are mainly related to the periods of the annular array fabricated therein. For a metal plate of finite thickness, the generated CSPs propagate inside the annular aperture and experience multiple reflections at both end-facets, hence forming Fabry–Pérot resonances in the cylindrical cavity. On resonance, the condition $|2Lk_{SPP}(\omega) + \Delta\phi_1 + \Delta\phi_2| = 2m\pi$ is satisfied,[33] with L the thickness of the metal film, $k_{SPP}(\omega)$ the wave vector of the CSP at frequency of ω, $\Delta\phi_{1,2}$ the phase shift as a result of CSP reflection at either facet of the cavity, and m the mode number. The CSP-induced transmission peak is a direct result of the Fabry–Pérot resonances. Additionally, the PSPs related to the period of the annular array also play an important role for the selective transmission. The PSP-induced transmission peak can be approximately estimated as $\lambda_{max} = \left(\Lambda/\sqrt{n_x^2 + n_y^2}\right)\sqrt{\varepsilon_d\varepsilon_m/(\varepsilon_d + \varepsilon_m)}$,[46] where ε_d and ε_m are the dielectric functions of the dielectric and the metal, respectively, Λ is the lattice constant of the array, and n_x and n_y are integers. In our case, the transmission peaks in the range of 500–600 nm in the simulation indeed satisfy the above expression for a ±(1, 1) mode at the Au/LC interface, while the ones in the range of 700–800 nm are attributed to the CSP. In addition, from Figure 4a and b, at a smaller aperture size, the CSP-induced transmission peak intensity is higher than the PSP-induced one. As the aperture size increases, PSP-induced transmission gradually plays a dominant role, moreover, the full width at half maximum (FWHM) also increases and finally saturates, as shown in the inset of Figure 4b. Figure 4c plots the peak positions of the transmission as a function of aperture size, which are retrieved from both calculated (Figure 4a) and experimental data (Figure 4b). It is clear from calculation that the PSP-induced transmission peak linearly red-shifts while

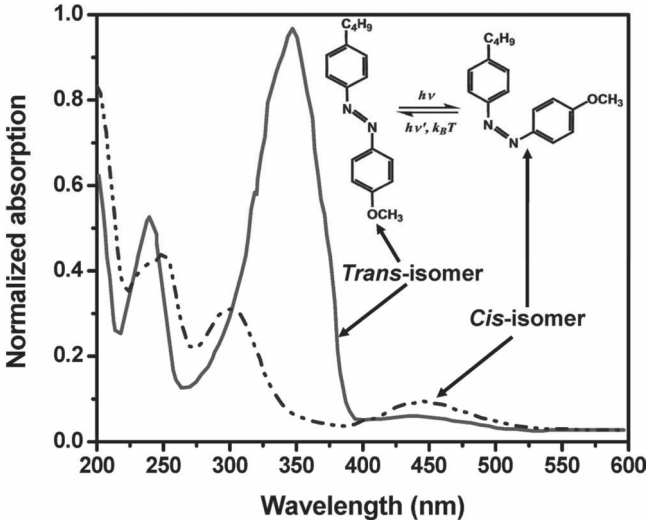

Figure 2. The *trans–cis* isomerization of BMAB under the UV flood exposure. The inset shows the chemical structure of a BMAB molecule and its reversible *trans–cis* isomerization.

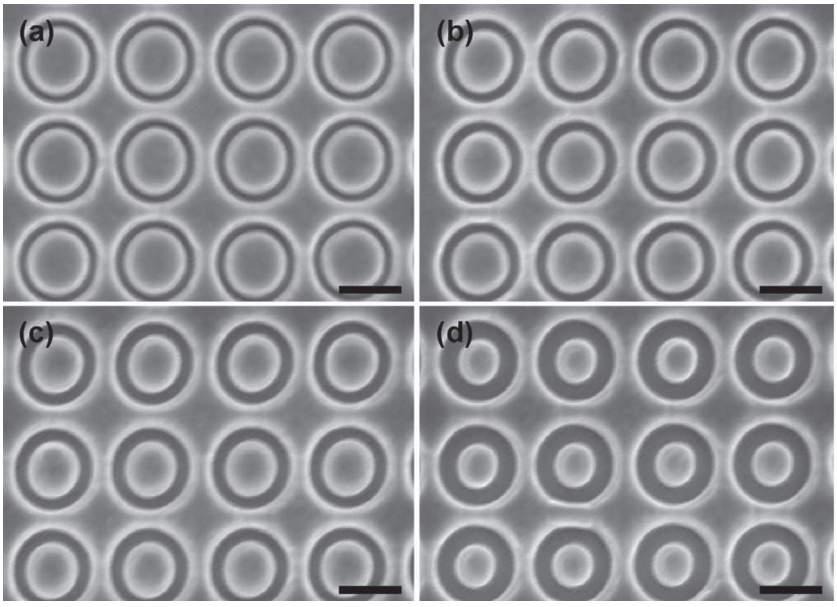

Figure 3. Typical scanning electron microscope images showing the Au AAAs with the aperture size of a) 40 nm, b) 80 nm, c) 100 nm, and d) 140 nm, respectively, by varying the inner radius. The outer radius was fixed at 320 nm. The period of the AAAs was 800 nm for all cases. Scale bar: 500 nm.

the CSP-induced transmission peak linearly blue-shifts with an increase of aperture size. The red-shift of the PSP-induced peaks can be attributed to the cutoff behavior. In our design, we fixed the lattice constant at 800 nm and the outer radius at 320 nm. As the inner radius decreases, the annular aperture size increases. The resulting increase in transmission will be larger for longer wavelengths than for shorter wavelengths, since transmission beyond cutoff has a nonlinear dependence on wavelength. This effectively leads to a red-shift as the aperture size increases. The observed increase in the width of the transmitted peaks with increasing aperture size is consistent with recent observations that the radiative damping of the SPPs increases with hole size.[47] For AAAs, Haftel et al. have theoretically investigated the role of CSPs in enhanced optical transmission and found that the resonant CSP wavelength increases as the annular aperture size decreases.[48] Our calculation results clearly confirmed a similar trend. It is worth mentioning that for the PSP-induced peaks, the calculated and experimental data follow a general trend although there is a slight offset, while for the CSP-induced peaks, the experimental results deviate largely from the calculated data. This discrepancy between calculated and experimental results for CSP-induced peaks could be attributed to non-ideal aperture profiles due to fabrication imperfections, such as re-deposition and charging effects. Figure 4d shows the CCD captured colors for the corresponding structures under an optical microscope. We can see from Figure 4d that the color changes from bluish to reddish as the aperture size increases except for the aperture size of 20 nm, which shows a carmine color because the CSP-induced transmission at 700–800 nm dominates, as seen from Figure 4b. From Figure 4b, the PSP- and CSP-induced peaks are not completely overlapped, hence resulting in a relatively high color cross-talk. As a result, the filtered colors were washed out. However, from the calculation (see Figure 4c), it is possible to make the PSP- and CSP-induced peaks overlap completely by carefully designing the structure, which in principle gives the best performance of the color filters. In addition, the addition of the LC overlayer generally induces a large red-shift compared to the bare gold AAAs. Although it is still possible to produce the blue color by decreasing the period of gold AAAs, the ease of fabrication may become an issue. In this sense, silver and aluminum could be another choice to achieve the blue color filters since they have higher plasma frequencies compared to gold.

For the azobenzene-based optical materials, a distinct advantage is that they can be optically controlled, an important factor in developing all-optical devices. We investigated the dynamic changes of transmission for color filters. **Figure 5** shows a typical evolution of the transmission spectra as a function of time under the UV pump for the AAA with an aperture size of 120 nm. We can see that the transmission peak intensity decreases with an increase of the pump time. When the BMAB absorbs UV light, the *trans*-isomer transforms into the *cis*-isomer. The *cis*-isomer affects the host nematic as an impurity, disrupting the local order and forming an isotropic phase. This order change generates a photoinduced refractive index modulation. As known, the plasmonic effect only happens in a localized area (generally less than 100 nm) near the dielectric/metal interface.[49] The alignment of the LC molecules inside and outside the annular aperture could play a significant role in photoinduced refractive index modulation, thus affecting the transmittance of the whole device. Crawford et al. have investigated the molecular-anchoring properties of the nematic LCs in cylindrical cavities and found that an escaped radial with singular point defects (ERPD) alignment was preferably supported for an untreated cavity with its radius larger than 50 nm.[50] We believe a similar alignment mechanism could happen inside the aperture. At the ERPD alignment inside the aperture, the effective refractive index of the LCs was approximated to be the same as the isotropic state for an unpolarized probe light. Outside the aperture, the LCs show the homogenous alignment (the magnified part I in Figure 1), demonstrating a nematic state. Although the LC domains are parallel to the substrate, they may rotate within the plane. Statistically, an unpolarized incoming beam will see an average of the ordinary and extraordinary indices. Therefore, the effective refractive index at the nematic state can be written as $n_{\mathrm{nem}} \cong \sqrt{(n_{\mathrm{o}}^2 + n_{\mathrm{e}}^2)/2} = 1.637$. As discussed, the *tans–cis* photoisomerization results in the N–I phase transition of LCs. As pump time increases, more and more BMAB *trans*-isomers transform into *cis*-isomers. The LCs become less and less nematic due to the disruption of long-range order. Ultimately, the LCs approach the isotropic state. At the isotropic state, the effective refractive index becomes $n_{\mathrm{iso}} \cong \sqrt{(2n_{\mathrm{o}} + n_{\mathrm{e}})/3} = 1.596$, a 0.041 decrease

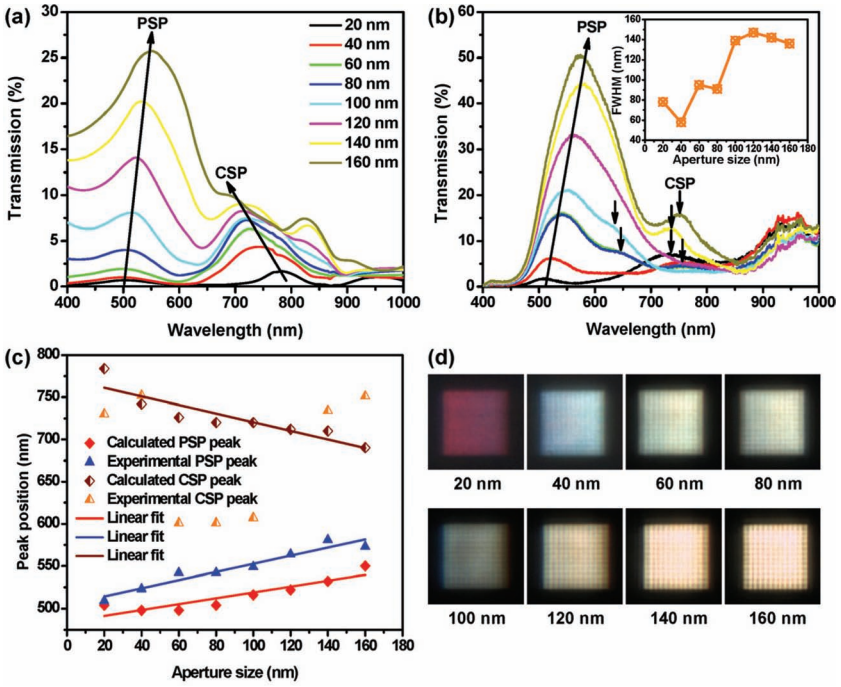

Figure 4. The theoretically calculated (a) and experimentally measured (b) transmission spectra of color filters with different aperture sizes, respectively. The inset in (b) shows the measured FWHM of corresponding transmission peaks. Panels (a) and (b) share the same legend. c) Peak positions of the transmission retrieved from calculated (a) and experimental (b) data as a function of aperture size. d) CCD captured colors corresponding to the measured transmission spectra (b) under an optical microscope.

in refractive index compared to n_{nem}. As a result, we observed a ~18% decrease in the peak transmission intensity due to photoinduced refractive index modulation. Note that only a slight decrease of refractive index resulted in a significant modulation of transmission intensity in our experiment. It is therefore expected that the modulation depth could be further enhanced by using a LC with a larger birefringence.

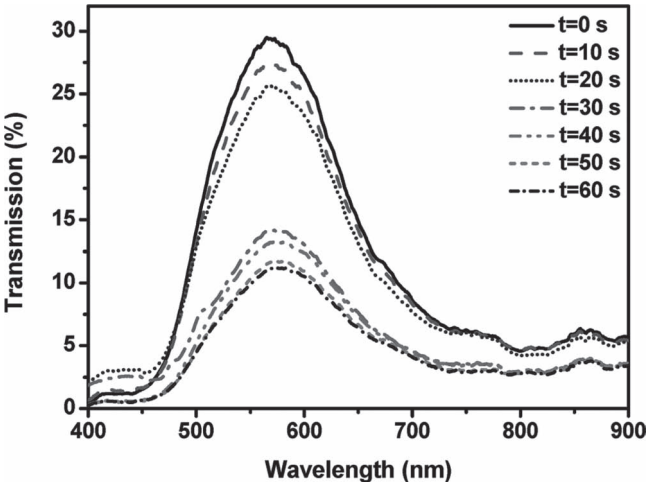

Figure 5. The evolution of the transmission spectra as a function of time under the UV pump for the color filter with an aperture size of 120 nm.

In conclusion, we have demonstrated light-driven plasmonic color filters by integrating gold AAAs with photoresponsive LCs. The light-excited PSPs and CSPs play a collective role in their transmission properties. PSP-induced transmission gradually plays a dominant role as the aperture size increases. This device demonstrates an all-optical modulation of the transmission intensity due to the *trans–cis* photoisomerization-induced N–I phase transition of the LCs. The all-optical tuning behavior is highly reversible and reproducible. Our future work includes developing red, green, and blue plasmonic color filters with optimized performance. We expect that with such three color filters, any color could be achieved by optically controlling their compositions, thus advancing information displays.

Experimental Section

To fabricate the gold AAAs, a Ti adhesion layer (3 nm) and a Au layer (110 nm) were subsequently deposited on a quartz substrate by electron-beam evaporation (EDWARDS Auto 306 Turbo E-beam Evaporator). Dense coaxial AAAs were then fabricated using focused ion beam (FIB) milling (FIB 200, FEI Company). To minimize re-deposition effects, all patterns were milled in parallel instead of serial. A probe current of 70 pA was applied with a 30 kV acceleration voltage during the FIB milling process. A set of AAAs were fabricated with a varying inner radius, r_{in}, from 300 nm to 160 nm in a step of 20 nm, and all with a fixed outer radius of r_{out} = 320 nm. The period of all the arrays was fixed at 800 nm.

To apply a LC layer on the AAAs, a cell was formed by assembling two substrates: one was a quartz substrate with AAAs and the other one was an indium–tin–oxide (ITO) glass substrate coated with a rubbed polyimide (PI) alignment layer. The cell thickness was controlled to be ~7 μm using the polystyrene microbeads. The LC material used in our experiments consisted of 87.3 wt% nematic LC, E7 (Merck), and 12.7 wt% photochromic LC, BMAB, which were mechanically mixed at an elevated temperature of 70 °C to form a homogenous mixture. The LC E7 serves as a host material, which has an ordinary refractive index of n_o = 1.521 and an extraordinary refractive index of n_e = 1.746, giving a birefringence of Δn = 0.225 (all at λ = 589 nm). BMAB has a liquid crystalline behavior with a nematic–isotropic (N–I) phase transition temperature at T_{NI}(BMAB) = 45 °C. The homogeneous mixture was infiltrated into the LC cell by capillary action. After infiltration of LCs, a roughly homogeneous alignment of LCs was expected, i.e., LC molecules aligned parallel to the substrates, due to the fact that the alignment layer on the ITO glass substrate caused a preferred alignment across the cell through the van der Waals force between LC molecules.

The optical transmission properties were modelled using the finite-difference time-domain method (FDTD, Lumerical). A unit cell of the structure was simulated with periodic boundary conditions in the *x*–*y* direction and perfectly matched layer (PML) boundary condition in the *z* direction. We injected a plane wave with polarization direction along the *x* axis from the bottom of the quartz substrate. The dispersion of gold was based on the Johnson and Christy model[51] in the material library of the software and that of LC E7 was derived by fitting the experimental data using a three-coefficient Cauchy model.[52] In our experiments, optical

transmission spectra were measured with an unpolarized probe light beam using a UV–vis–NIR microspectrophotometer (CRAIC QDI 2010). The probe light beam was focused to have a detecting area of 7.1 × 7.1 μm^2 using a 36× objective lens combined with a variable aperture. The dynamic spectral change was achieved when the device was subject to the pump light: a flood exposure using a UV light source (ELC-410). The enlarged part I shows the schematic view of the gold AAA pattern.

Supporting Information

Supporting Information is available from the Wiley Online Library or from the author.

Acknowledgements

This work was financially supported by Agency for Science, Technology and Research (A*STAR), under the grant No. 0921540099 and 0921540098. GYS and NX also thank the funding from Singapore Ministry of Education under the grant No. MOE2009-T2-1-086.

Received: November 21, 2011
Revised: December 13, 2011
Published online: March 21, 2012

[1] H. Raether, *Surface Plasmons on Smooth and Tough Surfaces and on Gratings*, Springer, Berlin **1988**.
[2] M. Quinten, A. Leitner, J. R. Krenn, F. R. Aussenegg, *Opt. Lett.* **1998**, *23*, 1331.
[3] S. A. Maier, P. G. Kik, H. A. Atwater, S. Meltzer, E. Harel, B. E. Koel, A. A. G. Requicha, *Nat. Mater.* **2003**, *2*, 229.
[4] A. V. Krasavin, A. V. Zayats, *Appl. Phys. Lett.* **2010**, *97*, 041107.
[5] V. K. S. Hsiao, Y. B. Zheng, B. K. Juluri, T. J. Huang, *Adv. Mater.* **2008**, *20*, 3528.
[6] Y. J. Liu, Q. Z. Hao, J. S. T. Smalley, J. Liou, I. C. Khoo, T. J. Huang, *Appl. Phys. Lett.* **2010**, *97*, 091101.
[7] T. Ming, L. Zhao, M. D. Xiao, J. F. Wang, *Small* **2010**, *6*, 2514.
[8] N. Fang, H. Lee, C. Sun, X. Zhang, *Science* **2005**, *308*, 534.
[9] Z. Liu, H. Lee, Y. Xiong, C. Sun, X. Zhang, *Science* **2007**, *315*, 1686.
[10] W. Srituravanich, L. Pan, Y. Wang, C. Sun, D. B. Bogy, X. Zhang, *Nat. Nanotechnol.* **2008**, *3*, 733.
[11] Y. H. Zhao, S. S.-C. Lin, A. A. Nawaz, B. Kiraly, Q. Z. Hao, Y. J. Liu, T. J. Huang, *Opt. Express* **2010**, *18*, 23458.
[12] P. Muhlschlegel, H.-J. Eisler, O. J. F. Martin, B. Hecht, D. W. Pohl, *Science* **2005**, *308*, 1607.
[13] W. Zhang, L. Huang, C. Santschi, O. J. F. Martin, *Nano Lett.* **2010**, *10*, 1006.
[14] D. Dregely, R. Taubert, J. Dorfmuller, R. Vogelgesang, K. Kern, H. Giessen, *Nat. Commun.* **2011**, *2*, 267.
[15] J. Dorfmuller, D. Dregely, M. Esslinger, W. Khunsin, R. Vogelgesang, K. Kern, H. Giessen, *Nano Lett.* **2011**, *11*, 2819.
[16] D. J. Bergman, M. I. Stockman, *Phys. Rev. Lett.* **2003**, *90*, 027402.
[17] J. Seidel, S. Grafstrom, *L. Eng, Phys. Rev. Lett.* **2005**, *94*, 177401.
[18] M. A. Noginov, G. Zhu, M. Mayy, B. A. Ritzo, N. Noginova, V. A. Podolskiy, *Phys. Rev. Lett.* **2008**, *101*, 226806.
[19] N. I. Zheludev, S. L. Prosvirnin, N. Papasimakis, V. A. Fedotov, *Nat. Photon.* **2008**, *2*, 351.
[20] T. W. Ebbesen, H. J. Lezec, H. F. Ghaemi, T. Thio, P. A. Wolff, *Nature* **1998**, *391*, 667.
[21] E. Ozbay, *Science* **2006**, *311*, 189.
[22] Y. J. Liu, Y. B. Zheng, J. Liou, I.-K. Chiang, I. C. Khoo, T. J. Huang, *J. Phys. Chem. C* **2011**, *115*, 7717.
[23] C. Genet, T. W. Ebbesen, *Nature* **2007**, *445*, 39.
[24] H. S. Lee, Y. T. Yoon, S. S. Lee, S. H. Kim, K. D. Lee, *Opt. Express* **2007**, *15*, 15457.
[25] D. Inoue, A. Miura, T. Nomura, H. Fujikawa, K. Sato, N. Ikeda, D. Tsuya, Y. Sugimoto, Y. Koide, *Appl. Phys. Lett.* **2011**, *98*, 093113.
[26] T. Xu, H. Shi, Y.-K. Wu, A. F. Kaplan, J. G. Ok, L. J. Guo, *Small* **2011**, *7*, 3128.
[27] K. Diest, J. A. Dionne, M. Spain, H. A. Atwater, *Nano Lett.* **2009**, *9*, 2579.
[28] T. Xu, Y.-K. Wu, X. G. Luo, L. J. Guo, *Nat. Commun.* **2010**, *1*, 59.
[29] E. S. P. Leong, Y. J. Liu, B. Wang, J. H. Teng, *ACS Appl. Mater. Interfaces* **2011**, *3*, 1148.
[30] E. Laux, C. Genet, T. Skauli, T. W. Ebbesen, *Nat. Photon.* **2008**, *2*, 161.
[31] F. I. Baida, D. Van Labeke, *Phys. Rev. B* **2003**, *67*, 155314.
[32] F. I. Baida, A. Belkhir, D. Van Labeke, O. Lamrous, *Phys. Rev. B* **2006**, *74*, 205419.
[33] R. de Waele, S. P. Burgos, A. Polman, H. A. Atwater, *Nano Lett.* **2009**, *9*, 2832.
[34] H. A. Atwater, A. Polman, *Nat. Mater.* **2010**, *9*, 205.
[35] S. P. Burgos, R. de Waele, A. Polman, H. A. Atwater, *Nat. Mater.* **2010**, *9*, 407.
[36] R. de Waele, S. P. Burgos, H. A. Atwater, A. Polman, *Opt. Express* **2010**, *18*, 12770.
[37] W. Fan, S. Zhang, B. Minhas, K. J. Malloy, S. R. J. Brueck, *Phys. Rev. Lett.* **2005**, *94*, 033902.
[38] G. Y. Si, Y. H. Zhao, H. Liu, S. L. Teo, M. S. Zhang, T. J. Huang, A. J. Danner, J. H. Teng, *Appl. Phys. Lett.* **2011**, *99*, 033105.
[39] J. Zhang, J.-Y. Ou, N. Papasimakis, Y. Chen, K. F. MacDonald, N. I. Zheludev, *Opt. Express* **2011**, *19*, 23279.
[40] P. A. Kossyrev, A. Yin, S. G. Cloutier, D. A. Cardimona, D. Huang, P. M. Alsing, J. M. Xu, *Nano Lett.* **2005**, *5*, 1978.
[41] W. Dickson, G. A. Wurtz, P. R. Evans, R. J. Pollard, A. V. Zayats, *Nano Lett.* **2008**, *8*, 281.
[42] Y. J. Liu, Y. B. Zheng, J. J. Shi, H. Huang, T. R. Walker, T. J. Huang, *Opt. Lett.* **2009**, *34*, 2351.
[43] Y. J. Liu, X. Y. Ding, S.-C. S. Lin, J. J. Shi, I.-K. Chiang, T. J. Huang, *Adv. Mater.* **2011**, *23*, 1656.
[44] Y. J. Liu, E. S. P. Leong, B. Wang, J. H. Teng, *Plasmonics* **2011**, *6*, 659.
[45] K. G. Yager, C. J. Barrett, *J. Photochem. Photobiol. A* **2006**, *182*, 250.
[46] H. F. Ghaemi, T. Thio, D. E. Grupp, T. W. Ebbesen, H. J. Lezec, *Phys. Rev. B* **1998**, *58*, 6779.
[47] D. S. Kim, S. C. Hohng, V. Malyarchuk, Y. C. Yoon, Y. H. Ahn, K. J. Yee, J. W. Park, J. Kim, Q. H. Park, C. Lienau, *Phys. Rev. Lett.* **2003**, *91*, 143901.
[48] M. I. Haftel, C. Schlockermann, G. Blumberg, *Phys. Rev. B* **2006**, *74*, 235405.
[49] A. J. Haes, C. L. Haynes, A. D. McFarland, G. C. Schatz, R. P. Van Duyne, S. Zou, *MRS Bull.* **2005**, *30*, 368.
[50] G. P. Crawford, D. W. Allender, J. W. Doane, *Phys. Lett. A* **1992**, *45*, 8693.
[51] P. B. Johnson, R. W. Christy, *Phys. Rev. B* **1972**, *6*, 4370.
[52] J. Li, C.-H. Wen, S. Gauza, R. B. Lu, S.-T. Wu, *J. Display Technol.* **2005**, *1*, 51.